Measuring acoustic mode resonance alone as a sensitive technique to extract antiferromagnetic coupling strength

Yajun Wei* and Peter Svedlindh
Department of Engineering Sciences, Uppsala University, 751 21 Uppsala, Sweden

Mikhail Kostylev
Department of Physics, University of Western Australia, 6009 Crawley, Australia

Mojtaba Ranjbar, Randy K. Dumas, and Johan Åkerman
Department of Physics, University of Gothenburg, 412 96 Gothenburg, Sweden
(Received 11 May 2015; published 24 August 2015)

We have studied static and dynamic magnetic properties of a general asymmetric trilayer system using numerical simulations. For ferromagnetic, 90°, and antiferromagnetic coupling, the magnetizations of the two magnetic layers exhibit one, two, and three phases with increasing external field, respectively. The total magnetization and ferromagnetic resonance accordingly follow these phases of the magnetization vectors. The resonance condition is related to the interlayer coupling strength in such a way that a larger coupling constant yields a higher value of $f_{\rm res}/H$, where $f_{\rm res}$ is the resonance frequency at the external magnetic field H. Based on the simulation results, it is proposed that measurements of the acoustic mode resonance alone at unsaturated conditions provide a sensitive and accurate technique to extract the antiferromagnetic coupling strength. The technique is demonstrated experimentally with the broadband ferromagnetic resonance measurements of two trilayer films with weak and strong coupling strengths. The technique offers an efficient and sensitive method for antiferromagnetic coupling strength extraction, yielding coupling constant values with a precision of better than 0.03 erg/cm^2. Also, separation of the bilinear and biquadratic coupling contributions is possible with the technique.

DOI: 10.1103/PhysRevB.92.064418 PACS number(s): 75.70.−i, 76.50.+g, 68.65.−k, 76.20.+q

I. INTRODUCTION

A nanometer thick trilayer system with two ferromagnetic (FM) layers separated by a nonmagnetic (NM) spacer layer is an elementary building block of magnetic devices with various technological applications such as magnetic recording devices, magnetic sensors, nonvolatile magnetic random memories, and spin-torque oscillators [1–4]. Understanding the influence of material parameters such as magnetic anisotropy, saturation magnetization, and interlayer coupling on the magnetic response of the trilayer system to an external field is of critical importance for the engineering of FM/NM/FM trilayer based magnetic devices [5,6]. Therefore, following the discovery of the interlayer coupling [7] and its oscillatory dependence with respect to the thickness of the nonmagnetic spacer [8] trilayer systems have attracted immense research interest [9,10].

Most of the investigations have been carried out on symmetrical trilayers with the two FM layers made from the same material [11–14]. But recently, experimental studies of trilayers with the two FM layers made from different materials have appeared [15–17]. To date, systematic numerical analysis of the static and dynamic magnetic responses of an asymmetrical trilayer with the two FM layers composed of different materials are rare. In this paper we present results on the influence of interlayer coupling on the static and dynamic magnetic properties of a general asymmetric trilayer system obtained by numerical simulations. Static magnetization curves and ferromagnetic resonance (FMR) dispersion relations are calculated for different coupling types and strengths. Many interesting features are found from the simulated results, which are valuable references for experimental work.

Specifically, it is known that the optic mode resonance is very difficult to observe in FMR studies of antiferromagnetically coupled trilayers [18,19]. The results of this study indicate that the acoustic branch of the ferromagnetic resonance dispersion curve is sensitive to the coupling strength before reaching magnetic saturation, corresponding to the magnetization of both FM layers being aligned with external magnetic field, in antiferromagnetically coupled trilayers. Therefore, measuring only the acoustic mode resonance at unsaturated conditions for different microwave frequencies is proposed and experimentally demonstrated as a sensitive and accurate technique to extract the coupling strength for antiferromagnetically coupled trilayers.

II. MACROSPIN MODEL

In a trilayer system, besides the Zeeman energy, anisotropic energy, and demagnetizing energy, there is an additional energy term, an exchange energy stemming from the interlayer exchange coupling, which is given by

$$\varepsilon_{\rm ex} = -J_1 \frac{\vec{M}_{\rm A}\cdot\vec{M}_{\rm B}}{M_{\rm A}M_{\rm B}} - J_2\left(\frac{\vec{M}_{\rm A}\cdot\vec{M}_{\rm B}}{M_{\rm A}M_{\rm B}}\right)^2, \qquad (1)$$

where $\vec{M}_{\rm A}$ and $\vec{M}_{\rm B}$ are the magnetization vectors of the two FM layers. J_1 is the bilinear coupling constant, and J_2 is the biquadratic coupling constant, both given in units erg/cm^2.

We consider a trilayer system with two FM layers of the same thickness t separated by a NM spacer with thickness $t_{\rm NM}$. The geometry and coordinate system employed in the study are shown in Fig. 1. Taking into account the Zeeman energy

*yajun.wei@angstrom.uu.se

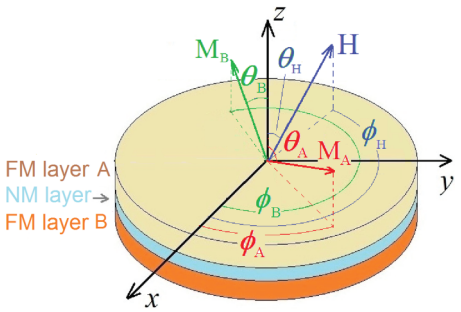

FIG. 1. (Color online) The geometry and coordinate system of the film.

ε_{zee}, exchange energy ε_{ex}, and demagnetizing energy ε_{dem}, the total energy per unit area of the system is

$$\begin{aligned}\varepsilon_{tot} &= \varepsilon_{zee} + \varepsilon_{ex} + \varepsilon_{dem}\\ &= -tHM_A[\sin\theta_H \sin\theta_A\cos(\phi_H-\phi_A)+\cos\theta_H\cos\theta_A]\\ &\quad - tHM_B[\sin\theta_H \sin\theta_B\cos(\phi_H-\phi_B)+\cos\theta_H\cos\theta_B]\\ &\quad - J_1[\sin\theta_A \sin\theta_B\cos(\phi_A-\phi_B)+\cos\theta_A\cos\theta_B]\\ &\quad - J_2[\sin\theta_A \sin\theta_B\cos(\phi_A-\phi_B)+\cos\theta_A\cos\theta_B]^2\\ &\quad + 2\pi t\left(M_A^2\cos^2\theta_A + M_B^2\cos^2\theta_B\right). \end{aligned} \tag{2}$$

θ_A, θ_B, ϕ_A, and ϕ_B correspond to the polar and azimuth angles of the magnetization vectors, as indicated in Fig. 1. H, θ_H, and ϕ_H refer to the magnitude, polar angle, and azimuth angle of the external magnetic field, respectively.

If J_1 dominates over J_2, a positive value of J_1 will lead to the system favoring a parallel configuration of the two magnetization vectors in order to minimize the exchange coupling energy. Therefore, a positive J_1 corresponds to ferromagnetic coupling. On the contrary, a negative J_1 will make the two magnetization vectors to align antiparallel with respect to each other to minimize their exchange energy, corresponding to antiferromagnetic coupling [20]. However, if J_2 dominates over J_1 and is positive, minimum energy occurs when the two magnetizations are oriented perpendicularly to each other (90° coupling).

For a given set of parameters characterizing the trilayer system (J_1, J_2, M_A, and M_B), the equilibrium orientations of the magnetizations at any external field can be calculated numerically by finding the values of θ_A, θ_B, ϕ_A, and ϕ_B that minimize ε_{tot}. Using these values, the in-plane static magnetization of the system can be obtained as

$$\begin{aligned} m_\parallel &= \frac{M_\parallel(H)}{M_s}\\ &= \frac{M_A\sin\theta_A\cos\phi_A(H) + M_B\sin\theta_B\cos\phi_B(H)}{M_A+M_B} \end{aligned} \tag{3}$$

and the out-of-plane static magnetization of the film is given by

$$\begin{aligned} m_\perp &= \frac{M_\perp(H)}{M_s}\\ &= \frac{M_A\cos\theta_A(H) + M_B\cos\theta_B(H)}{M_A+M_B}. \end{aligned} \tag{4}$$

Ferromagnetic resonance (FMR) experiments use a microwave signal generating an rf magnetic field $\vec{h}$ that is perpendicular to the dc field. Resonance absorption occurs when the microwave frequency matches the natural frequency of the system, which is determined by the magnetic properties of the sample and the dc magnetic field. By substituting the total energy density [Eq. (2)] and the equilibrium angles into the Suhl-Smit equation [21] the resonance condition is obtained as a fourth order polynomial equation of the microwave angular frequency ω, which reads

$$a\omega^4 + c\omega^2 + e = 0. \tag{5}$$

The coefficients of this fourth order polynomial equation are

$$\begin{aligned} a &= \left(\frac{t^2M_AM_B}{\gamma_A\gamma_B}\right)^2,\\ c &= -t^2M_AM_B\left[\left(\frac{h_1^Ah_2^A}{\gamma_B^2}+\frac{h_1^Bh_2^B}{\gamma_A^2}\right)+\frac{2C_0C_2}{\gamma_A\gamma_B}\right.\\ &\quad + C_1\left(\frac{tM_Ah_2^B}{\gamma_A^2}+\frac{tM_Bh_2^A}{\gamma_B^2}\right)+C_2\left(\frac{tM_Ah_1^B}{\gamma_A^2}+\frac{tM_Bh_1^A}{\gamma_B^2}\right)\\ &\quad \left.+C_1C_2\left(\frac{M_A}{M_B\gamma_A^2}+\frac{M_B}{M_A\gamma_B^2}\right)\right],\\ e &= \left[t^2M_AM_B + C_2\left(tM_Ah_2^A+tM_Bh_2^B\right)\right]\\ &\quad \times\left[t^2M_AM_Bh_1^Ah_1^B + C_1\left(tM_Ah_1^A+tM_Bh_1^B\right)\right.\\ &\quad \left.+\left(C_1^2-C_0^2\right)\right], \end{aligned} \tag{6}$$

with γ_A and γ_B being the gyromagnetic ratio of the FM layer A and B, respectively. The parameters in Eq. (6) are defined as

$$\begin{aligned} C_0 &= J_1 + 2J_2\cos(\phi_A-\phi_B),\\ C_1 &= J_1\cos(\phi_A-\phi_B) + 2J_2\cos^2(\phi_A-\phi_B),\\ C_2 &= J_1\cos(\phi_A-\phi_B) + 2J_2\cos 2(\phi_A-\phi_B), \end{aligned} \tag{7}$$

and

$$\begin{aligned} h_1^A &= H\cos\phi_A + 4\pi M_A,\\ h_1^B &= H\cos\phi_B + 4\pi M_B,\\ h_2^A &= H\cos\phi_A,\\ h_2^B &= H\cos\phi_B. \end{aligned} \tag{8}$$

Among the four solutions to Eq. (5), only two are physically meaningful. These two solutions are referred to as the acoustic resonant mode, which corresponds to the magnetization vectors of the FM layers precessing in-phase and the optic resonant mode, which corresponds to the two magnetization vectors precessing 180° out-of-phase. Therefore, one would expect two distinct resonance peaks to appear in the FMR spectrum. In the case when the two FM layers are identical, the resonance field difference of the two modes corresponds to the value of the exchange field.

III. SIMULATED RESULTS

Figures 2 and 3 present some simulated curves for ferromagnetically and antiferromagnetically coupled trilayers,

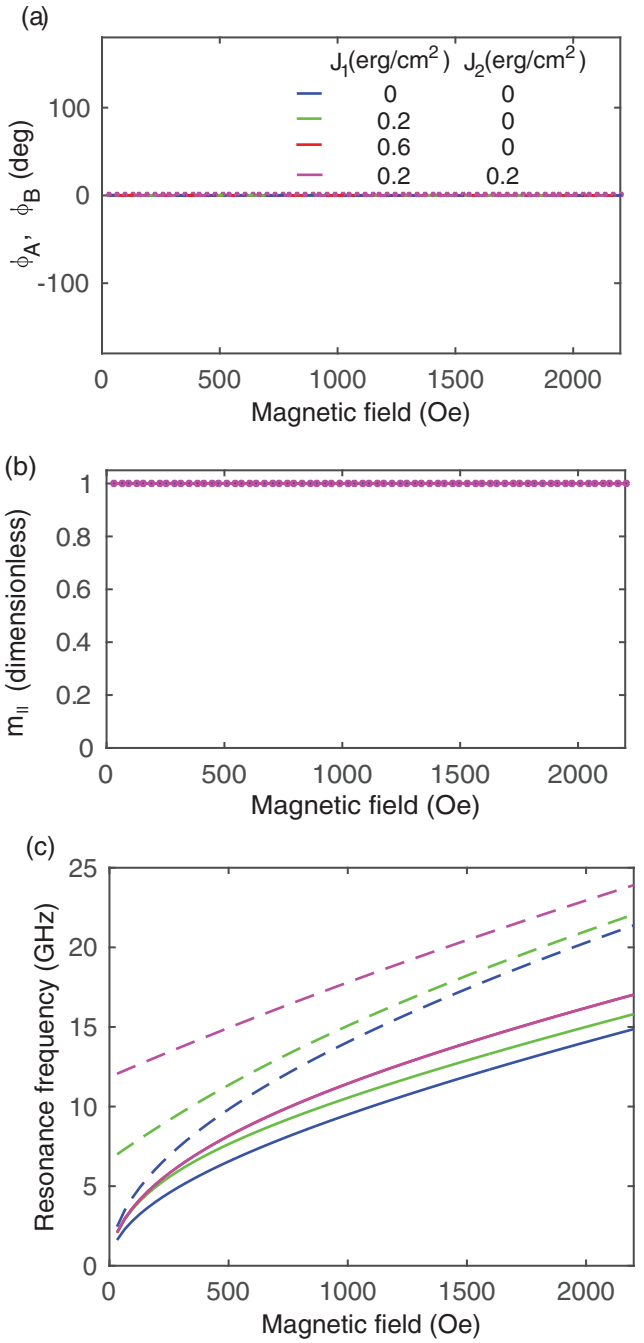

FIG. 2. (Color online) Simulated results of magnetization orientations ϕ_A and ϕ_B (a), magnetization (b), and FMR resonance frequency (c) versus in-plane magnetic field for different coupling strengths. The magnetization values of the two FM layers are $4\pi M_A = 22$ kG and $4\pi M_B = 9.5$ kG. Different coupling constants are represented by different colors of the curves, with the legend shown in (a). Solid and dashed lines in (c) correspond to acoustic and optic mode resonance curves, respectively. The red curve is covered by the magenta one in (c) as they overlap with each other. In (a) and (b), curves for all four sets of coupling constants overlap.

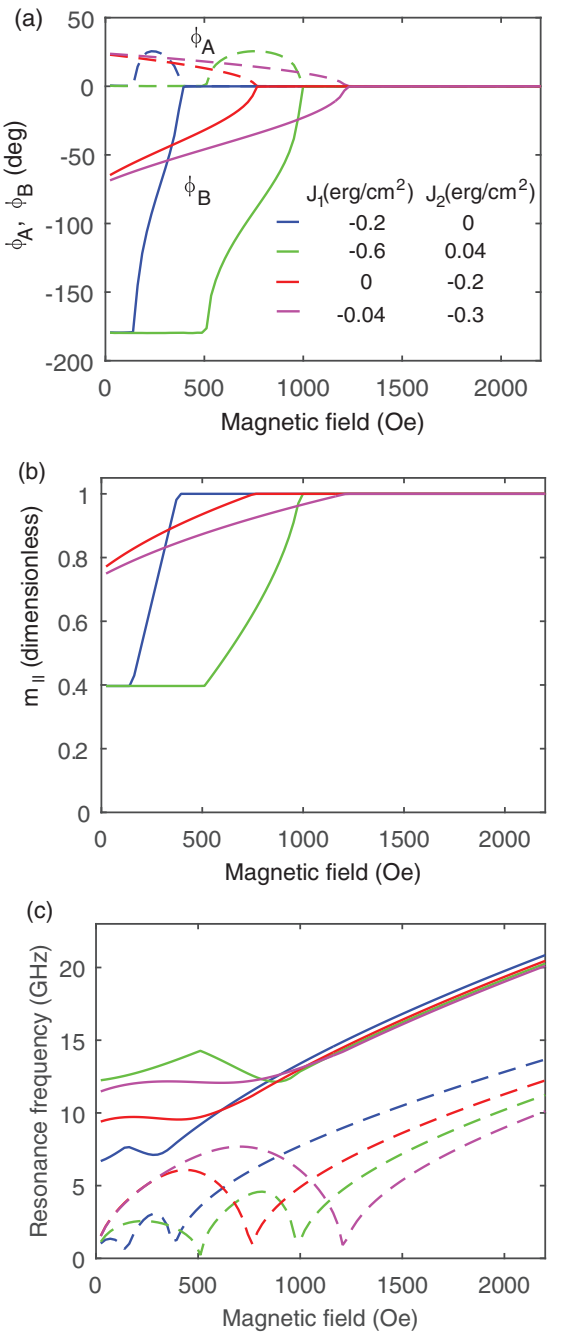

FIG. 3. (Color online) Simulated results of magnetization orientations ϕ_A and ϕ_B (a), magnetization (b), and FMR resonance frequency (c) versus in-plane magnetic field for different strengths of antiferromagnetic coupling. The magnetization values of the two FM layers are $4\pi M_A = 22$ kG and $4\pi M_B = 9.5$ kG. Different coupling constants are represented by different colors of the curves, with the legend shown in (a). In (c), the solid and dashed curves correspond to the acoustic and optic branches, respectively, of the dispersion relation.

respectively. From the figures, many features expected to be observed in FMR studies on trilayer systems can be seen.

A. Ferromagnetic coupling

For ferromagnetic coupling, as can be seen from Fig. 2(a), the two magnetizations are always aligned in parallel with the dc magnetic field. The in-plane magnetization is saturated, regardless of magnetic field and exchange coupling

magnitudes (neglecting magnetocrystalline anisotropy), as demonstrated by Fig. 2(b). In a decoupled system (i.e., very thick spacer layer), the FMR dispersion relation is described by a distinct Kittel formula for each layer, as shown by the blue curve in Fig. 2(c).

In a FM coupled trilayer, the optic branch of the dispersion curve is significantly pushed to higher frequencies. The two resonance conditions for a FM coupled trilayer system are both dependent on the strength of the coupling in such a way that a stronger coupling leads to a higher value of $f_{\rm res}/\gamma H$, where $f_{\rm res}$ is the resonance frequency at the magnetic field H. In other words, the resonance frequencies of both the acoustic and optic modes increase with increasing coupling in a frequency-swept FMR measurement at fixed dc magnetic field. While in a field-swept FMR measurement at fixed microwave frequency, the resonance fields of both modes decrease with increasing coupling strength. This is in agreement with experimental findings for trilayer films [20,22–24]. It is evident from Fig. 2(c) that the resonance condition of the optic branch is more sensitive to coupling strength than that of the acoustic branch. It is found that as the spacer thickness decreases, the optic mode resonance peak becomes broader and its intensity decreases [25].

As one can see from Eqs. (7) and (8), for ferromagnetically coupled films where $\phi_{\rm A} = \phi_{\rm B} = 0$, the contributions from J_1 and J_2 can no longer be separated. Therefore, the coupling strength is described by the effective coupling constant $J_{\rm eff} = J_1 + 2J_2$ [20]. This is demonstrated by the complete overlap of the red and magenta curves in Fig. 2(c).

Ultimately, in the case that the two FM layers are strongly coupled, the optic mode will disappear (or move to frequencies much higher than can be experimentally measured), leaving only the acoustic mode being observable [9]. In this case, only the equivalent effective magnetization and the equivalent gyromagnetic ratio of the whole system can be extracted by FMR, while the magnetic parameters of the individual layers cannot be separated. The in-plane resonance condition for an isotropic system in this case reads

$$\left(\frac{\omega}{\gamma_{\rm eqv}}\right)^2 = H[H - (4\pi M_{\rm eff})_{\rm eqv}], \tag{9}$$

where

$$\gamma_{\rm eqv} = \frac{4\pi M_{\rm A} + 4\pi M_{\rm B}}{4\pi M_{\rm A}/\gamma_{\rm A} + 4\pi M_{\rm B}/\gamma_{\rm B}} \tag{10}$$

and

$$(4\pi M_{\rm eff})_{\rm eqv} = (4\pi M_s)_{\rm eqv} - H_{\rm p,eqv}, \tag{11}$$

with the equivalent saturation magnetization $(4\pi M_s)_{\rm eqv}$ and equivalent perpendicular anisotropy field $H_{\rm p,eqv}$ being

$$(4\pi M_s)_{\rm eqv} = \frac{(4\pi M_{\rm A})^2 + (4\pi M_{\rm B})^2}{4\pi M_{\rm A} + 4\pi M_{\rm B}} \tag{12}$$

and

$$H_{\rm p,eqv} = \frac{H_{\rm p,A}(4\pi M_{\rm A}) + H_{\rm p,B}(4\pi M_{\rm B})}{4\pi M_{\rm A} + 4\pi M_{\rm B}}, \tag{13}$$

where $H_{\rm p,A}$ and $H_{\rm p,B}$ are the individual perpendicular anisotropy fields of layer A and B, respectively.

B. Antiferromagnetic coupling

In the case of antiferromagnetic coupling, the orientation of the magnetizations at equilibrium is more complicated than that of ferromagnetically coupled trilayers. The magnetization of each layer depends on the relative magnitude of the bilinear and biquadratic coupling constants. We discuss only two special cases for the sake of simplicity: $J_1 \gg J_2$ and $J_2 \gg J_1$.

When $J_2 \gg J_1$, the mutual angle between two magnetizations attains the value 90° at zero external field in order to minimize the energy of the system. With increasing dc magnetic field, the two magnetization vectors rotate towards the direction of the magnetic field, as shown in Fig. 3(a). There are two equilibrium phases of the magnetization vectors depending on the magnitude of the dc magnetic field with respect to the exchange field.

(1) When the magnetic field is smaller than the saturation field $H_{\rm sat}$, the magnetization vectors of both FMR layers will be at nonzero angles to the magnetic field direction.

(2) When the external field is larger than $H_{\rm sat}$, the magnetizations of both layers are aligned with the magnetic field.

The magnetization curve and dispersion relation also exhibit two phases, as indicated in Figs. 3(b) and 3(c) by the red and magenta curves. After magnetic saturation the acoustic mode resonance position becomes independent of coupling strength, while at an unsaturated condition both the acoustic and optic modes are quite sensitive to coupling strength. When the external field is larger than $H_{\rm sat}$, a stronger coupling yields a lower value of $f_{\rm res}/\gamma H$ for the optic mode. In other words, the resonance frequency of the optic mode decreases with increasing coupling strength in a frequency-swept FMR measurement, while in a field-swept FMR measurement, the resonance fields of both modes increase with increasing coupling strength.

When $J_1 \gg J_2$, the magnetizations of the two FM layers are aligned in antiparallel at zero magnetic field. In a magnetic field, there are three equilibrium phases of the magnetization vectors depending on the magnitude of the magnetic field with respect to the exchange field.

(1) When the magnetic field is smaller than a certain critical value $H_{\rm crit}$, the magnetizations in the two FM layers are aligned in antiparallel, due to the effect of the negative exchange coupling J_1. The total magnetization remains the same as at remanence.

(2) When the magnetic field is larger than $H_{\rm crit}$ but smaller than $H_{\rm sat}$, the magnetization vectors of both FMR layers will be at nonzero angles to the magnetic field direction.

(3) When the external field is larger than $H_{\rm sat}$, the magnetizations are aligned with the magnetic field.

The magnetization curve and dispersion relation also exhibit three distinct phases, as indicated in Figs. 3(b) and 3(c) by the blue and green curves. This result is in agreement with experimental and calculated results obtained by other researchers [19,26]. It is interesting to note that after magnetic saturation the acoustic mode resonance is only weakly dependent on the coupling strength, while at an unsaturated condition both the acoustic and optic modes are quite sensitive to coupling strength. When the external field is larger than $H_{\rm sat}$, the optic mode resonance condition for an AFM coupled trilayer is dependent on the strength of the

coupling in such a way that a stronger coupling leads to a lower value of $f_{res}/\gamma H$. In other words, the resonance frequency of the optic mode decreases with increasing coupling strength in a frequency-swept FMR measurement, while in a field-swept FMR measurement, the resonance fields of both modes increase with increasing coupling strength.

For the case when the two FM layers are strongly antiferromagnetically coupled, the optic mode resonance peak will also disappear (resonance shifts to very high frequency). Therefore, the trilayer system can also be treated as an equivalent single layer with its resonance condition identical to Eq. (9). But the definitions of equivalent effective magnetization $(4\pi M_{eff})_{eqv}$, equivalent gyromagnetic ratio γ_{eqv}, equivalent saturation magnetization $(4\pi M_s)_{eqv}$, and equivalent perpendicular anisotropy field $H_{p,eqv}$ are different and given by [9]

$$\gamma_{eqv} = \frac{4\pi M_A - 4\pi M_B}{4\pi M_A/\gamma_A + 4\pi M_B/\gamma_B}, \tag{14}$$

$$(4\pi M_{eff})_{eqv} = (4\pi M_s)_{eqv} - H_{p,eqv}, \tag{15}$$

$$(4\pi M_s)_{eqv} = \frac{(4\pi M_A)^2 + (4\pi M_B)^2}{4\pi M_A - 4\pi M_B}, \tag{16}$$

and

$$H_{p,eqv} = \frac{H_{p,A}(4\pi M_A) + H_{p,B}(4\pi M_B)}{4\pi M_A - 4\pi M_B}. \tag{17}$$

C. Discussion

It is important to make notice of the assumptions made in the macrospin model. Therefore, the results are valid only for isotropic trilayer films that are uniformly magnetized. In the experimental studies of realistic films, slight deviations from the simulated results are expected due to domain walls, interface contributions, and anisotropy energies. Nevertheless, the simple model reveals many interesting features of the magnetic response of trilayers.

IV. COUPLING STRENGTH EXTRACTION WITH ONLY ACOUSTIC MODE MEASUREMENTS

A. Background

Results from field dependent magnetization measurements can be used to determine the coupling constants of antiferromagnetically coupled trilayers. Theoretically, FMR is a more powerful technique because it can determine the coupling constants of either antiferromagnetically or ferromagnetically coupled trilayers. However, in an antiferromagnetically coupled trilayer, if the two ferromagnetic layers are identical, the optic mode will not be observed in the FMR spectrum due to the out-of-phase precession of the magnetizations that results in a destructive interference [18,19]. In a real trilayer film, there will be some differences between the two ferromagnetic layers implying that a low intensity optic resonance peak will in some cases be observed. Still, many researchers have found it difficult to observe the optic mode resonance [18,27–29].

In order to overcome this difficulty, a commonly used method is to make an asymmetrical structure (e.g., different layer thickness or different choice of material for the two FM layers) so that the effective magnetization of each ferromagnetic layer is different from one to the other [18,28]. However, the optic mode is still difficult to observe even in those cases, partly due to a broader linewidth and lower intensity for this mode [18,30]. This can be explained by the fact that the two FM layers might have different precession cone angles [31] making the time varying magnetization components along the transverse direction similar in size and opposite in direction in the optic mode resonance. Zhang *et al.* developed a technique called longitudinal pumping, which applies the rf field along the same direction as the dc magnetic field [32] to sense the optic mode. To detect both acoustic and optic modes, one needs to measure the FMR spectra twice, one with transverse pumping and the other with longitudinal pumping. In practice, this is not always easy to implement, especially for stripline FMR systems using a picoprobe station where the magnets are not easily made rotatable.

B. The technique with only acoustic mode measurements

An important implication from the results discussed in Sec. III B is that the observation of the optic mode resonance is not necessary in antiferromagnetically coupled samples if the purpose of the measurement is to determine the strength of the coupling. We noted that the acoustic mode resonance prior to magnetic saturation is quite sensitive to the coupling strength (see Fig. 3), which offers a possibility to extract the coupling constant by measuring only the acoustic mode dispersion relation. To do this, one needs to carry out measurements at many different magnetic fields at unsaturated conditions, which is not very practical with conventional FMR systems. Also, one may argue that field-swept measurements will not able to resolve a resonance spectrum as the equilibrium orientations of the magnetizations are gradually changing during the field sweep [33].

However, broadband vector network analyzer (VNA) based FMR measurements make this technique easily implementable. By employing a frequency-swept measurement at fixed field, one is able to lock the equilibrium orientations of the magnetizations to acquire microwave transmission or reflection spectra at different magnetic fields.

C. Experiment

To demonstrate the technique, we performed broadband frequency-swept FMR measurements on two trilayer samples with significantly different coupling constants. The trilayer samples have the structure of Si/SiO_2/FeNi(100 Å)/Ru(10 Å)/FeCo(100 Å)/Ta(30 Å) (referred to as sample S henceforth) and Si/FeCo(100 Å)/Ru(10 Å)/FeNi(100 Å)/Ru(10 Å) (referred to as sample L henceforth). The films were deposited at room temperature using dc magnetron sputtering with a base pressure of 5×10^{-8} Torr. The chemical composition of the FeNi and FeCo alloys are $Fe_{19}Ni_{81}$ and $Fe_{49}Co_{49}V_2$, respectively. A Helmholz coil was employed to enable measurements of FMR spectra at low fields. A VNA was used to measure frequency dependent S_{21} parameter of a coplanar waveguide (CPW) loaded with the sample within the frequency range of 1–20 GHz. A reference measurement with the unloaded CPW was subtracted as background. All measurements were performed at room temperature.

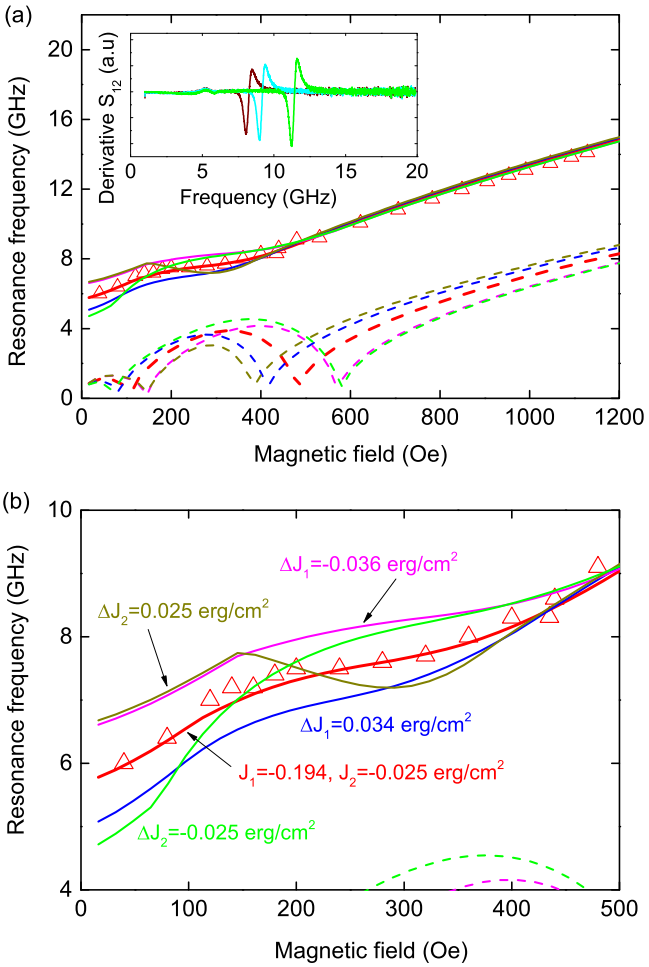

FIG. 4. (Color online) (a) FMR resonance frequency versus magnetic field for a Si/SiO_2/FeNi/Ru/FeCo/Ta trilayer with a Ru thickness of 10 Å. Circles correspond to experimental data and curves to simulated results with solid curves representing the acoustic branch dispersion relation and dashed curves the optic branch dispersion relation. The simulation parameters for FeNi layer are $4\pi M_{\mathrm{FeNi}} = 9.2$ kG and $g_{\mathrm{FeNi}} = 2.10$ and for FeCo layer are $4\pi M_{\mathrm{FeCo}} = 21$ kG and $g_{\mathrm{FeCo}} = 2.18$, measured using single layer thin films of each material in previous studies [17,34]. The inset shows three example FMR spectra measured with the magnetic fields 0.43 kOe (brown), 0.53 kOe (cyan), and 0.78 kOe (green). (b) A magnified view of (a) at unsaturated conditions. ΔJ_1 and ΔJ_2 refer to the deviation of coupling constants with respect to the best fitted J_1 and J_2 values (shown by the thick red curve).

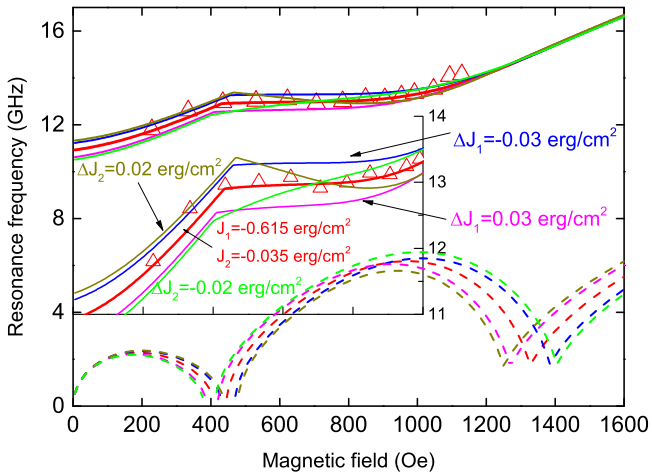

FIG. 5. (Color online) (a) FMR resonance frequency versus magnetic field for a Si/FeCo/Ru/FeNi/Ru trilayer with a Ru thickness of 10 Å. Circles correspond to experimental data and curves to simulated results with solid curves representing the acoustic branch dispersion relation and dashed curves the optic branch dispersion relation. The simulation parameters for FeNi layer are $4\pi M_{\mathrm{FeNi}} = 9.2$ kG and $g_{\mathrm{FeNi}} = 2.10$ and for FeCo layer are $4\pi M_{\mathrm{FeCo}} = 22$ kG and $g_{\mathrm{FeCo}} = 2.10$, measured using single layer thin films of each material in previous studies [17,35]. The inset shows a magnified view of the acoustic branch, with only the vertical axis zoomed. ΔJ_1 and ΔJ_2 refer to the deviation of coupling constants with respect to the best fitted J_1 and J_2 values (shown by the thick red curve).

D. Results and discussions

Figures 4 and 5 present the FMR results of sample S and sample L, respectively. Three typical FMR spectra of sample S are presented in the inset of Fig. 4(a) as examples. Apparently only the acoustic mode resonances are clearly observed. The solid and dashed lines in different colors correspond to calculated acoustic and optic branches of the dispersion relations using different coupling constants. From Fig. 4(b), which shows a magnified view of the acoustic branch fitting, one can see that the set of coupling constants $J_1 = -0.194$ and $J_2 = -0.025$ erg/cm^2 reproduces the experimentally measured data quite well and that a small variation of either J_1 or J_2 leads the simulated curves significantly deviating from the experimental data. One can safely say that the relative uncertainty of the measurement is less than 10%. Sample L exhibits stronger coupling, as the acoustic mode resonance frequencies are higher, shown in Fig. 5. The extracted coupling constants are $J_1 = -0.615$ and $J_2 = -0.035$ erg/cm^2. Again, an approximate 0.03 erg/cm^2 variation (5%) of the coupling constant results in an apparent deviation of the simulated curves, indicating a good sensitivity. Therefore, one can conclude that the precision of the technique is better than 0.03 erg/cm^2 (uncertainty <0.03 erg/cm^2). The coupling constant values are similar to those reported for FeNi/Ru/FeNi trilayers [20,36].

It is also worth noting from Fig. 4 that not only the acoustic branches but also the optic branches of the violet ($J_1 = -0.24$ erg/cm^2 and $J_2 = -0.025$ erg/cm^2) and green ($J_1 = -0.194$ erg/cm^2 and $J_2 = -0.05$ erg/cm^2) curves overlap because their effective coupling constants ($J_{\mathrm{eff}} = J_1 + 2J_2$) are almost equal. This indicates that for antiferromagnetically coupled trilayers, one must measure at unsaturated conditions to separate the contributions from bilinear J_1 and biquadratic J_2 coupling.

To further demonstrate the validity and accuracy of the technique, we compare the FMR results with their counterparts obtained by fitting the micromagnetic model to the experimental magnetization versus field data. Figure 6 exemplifies such a fitting for sample S, with the room temperature magnetization versus field data measured using a SQUID magnetometer shown as red circles and fitting curves shown as solid lines. The best fits yield the coupling constants $J_1 = -0.18$ erg/cm^2 and

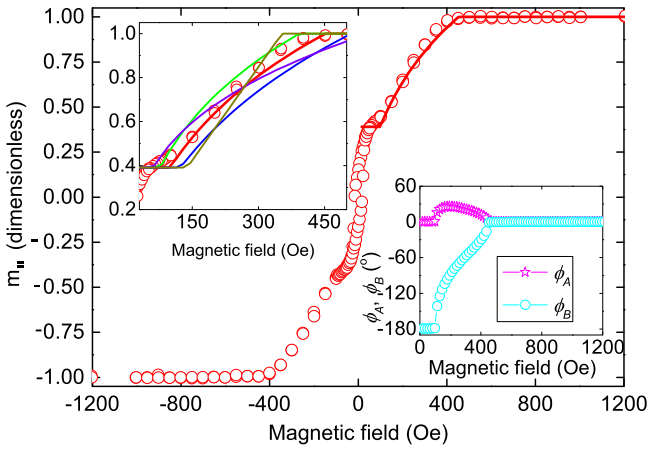

FIG. 6. (Color online) Magnetization versus magnetic field. Circles correspond to experimental data and the solid curve is a fit of the macrospin model to the experimental results yielding the coupling constants $J_1 = -0.18$ and $J_2 = -0.025$ erg/cm^2. The right bottom inset shows the angles between the magnetic field and the magnetizations in the FeCo (ϕ_A) and FeNi (ϕ_B) layers. The left top inset is a magnified view of the main graph at unsaturated conditions. A few attempts with different coupling constants are also shown in this inset, with the violet curve corresponding to $J_1 = -0.21$ erg/cm^2 and $J_2 = -0.025$ erg/cm^2, the blue one to $J_1 = -0.15$ erg/cm^2 and $J_2 = -0.025$ erg/cm^2, the green one to $J_1 = -0.18$ erg/cm^2 and $J_2 = -0.05$ erg/cm^2, and the olive one corresponding to $J_1 = -0.18$ erg/cm^2 and $J_2 = 0$ erg/cm^2.

$J_2 = -0.025$ erg/cm^2 for sample S and $J_1 = -0.57$ erg/cm^2 and $J_2 = -0.05$ erg/cm^2 for sample L. These values agree very well with the ones extracted from the acoustic mode FMR results. The fact that domain walls and multidomain states are not accounted for in the model most likely explains the discrepancies observed for the smallest fields. Also, comparing the inset of Fig. 6 with Fig. 4(b), one can see that the two techniques have similar precision (sensitivity) in determining the coupling constants.

V. SUMMARY

In summary, we systematically studied the static and dynamic magnetic responses of a general asymmetric trilayer system to dc magnetic field and microwave excitations using micromagnetic simulations. Many important features that are of large reference value to experimental work have been revealed. For the ferromagnetic coupling case, the equilibrium orientations of the magnetizations are always aligned with the magnetic field. For 90° coupling (J_2 dominated antiferromagnetic coupling), the equilibrium orientations of the magnetizations exhibit two phases with increasing external field, from the magnetization vectors of both FMR layers being at nonzero angles to the magnetic field direction to being aligned with the magnetic field. In the case of antiferromagnetic coupling (J_1 dominated antiferromagnetic coupling), the equilibrium orientations of the magnetizations exhibit three distinct phases with increasing external field, from antiparallel alignment to the magnetization vectors of both FMR layers being at nonzero angles to the magnetic field direction and finally to being aligned with the magnetic field. The total magnetization and ferromagnetic resonance accordingly follow these phases of the equilibrium orientations of the magnetization vectors. The resonance condition is related to the interlayer coupling strength in such a way that a stronger coupling yields a larger value of $f_{\rm res}/\gamma H$. For antiferromagnetic coupling and at saturated conditions, the optic mode resonance where the two magnetizations precess out-of-phase is sensitive to the coupling strength, while the acoustic mode where the two magnetizations precess in-phase is insensitive to the coupling strength. However, at unsaturated conditions, it is demonstrated, both numerically and experimentally, that measurements of the acoustic mode resonance alone provide a sensitive and accurate technique to extract the antiferromagnetic coupling strength. Unlike the traditional FMR technique that detects both the acoustic and optic mode resonances at magnetic saturation, this novel technique takes advantage of broadband FMR measurements and the feature that the acoustic mode resonance is sensitive to the coupling strength to enable extraction of their values without the need of including the optic mode resonances. Since the optic mode resonance is difficult to observe, this new technique offers an efficient and accurate alternative to probe the interlayer coupling of trilayer films. Also, it is possible to separate the bilinear and biquadratic contributions by using the technique.

ACKNOWLEDGMENTS

This work was supported by the Knut and Alice Wallenberg (KAW) Foundation and the Swedish Research Council (VR). The FMR measurements at the University of Western Australia (UWA) were supported by a Small Equipment Grant by UWA's Faculty of Science.

[1] J. Åkerman, Science **308**, 508 (2005).
[2] T. Kimura and M. Hara, Appl. Phys. Lett. **97**, 182501 (2010).
[3] M. Madami, S. Bonetti, G. Consolo, S. Tacchi, G. Carlotti, G. Gubbiotti, F. B. Mancoff, M. A. Yar, and J. Åkerman, Nat. Nanotechnol. **6**, 635 (2011).
[4] N. Locatelli, V. Cros, and J. Grollier, Nat. Mater. **13**, 11 (2014).
[5] R. L. Stamps, S. Breitkreutz, J. Åkerman, A. V. Chumak, Y. Otani, G. E. Bauer, J.-U. Thiele, M. Bowen, S. A. Majetich, M. Kläui *et al.*, J. Phys. D: Appl. Phys. **47**, 333001 (2014).
[6] T. M. Nakatani, S. Mitani, T. Furubayashi, and K. Hono, Appl. Phys. Lett. **99**, 182505 (2011).
[7] P. Grünberg, R. Schreiber, Y. Pang, M. B. Brodsky, and H. Sowers, Phys. Rev. Lett. **57**, 2442 (1986).
[8] S. S. P. Parkin, N. More, and K. P. Roche, Phys. Rev. Lett. **64**, 2304 (1990).
[9] A. Layadi, Phys. Rev. B **63**, 174410 (2001).
[10] M. Matczak, B. Szymański, M. Urbaniak, M. Nowicki, H. Głowiński, P. Kuświk, M. Schmidt, J. Aleksiejew, J. Dubowik, and F. Stobiecki, J. Appl. Phys. **114**, 093911 (2013).

[11] R. Gareev, V. Zbarsky, J. Landers, I. Soldatov, R. Schäfer, M. Münzenberg, H. Wende, and P. Grünberg, Appl. Phys. Lett. **106**, 132408 (2015).
[12] S. O. Demokritov, C. Bayer, S. Poppe, M. Rickart, J. Fassbender, B. Hillebrands, D. I. Kholin, N. M. Kreines, and O. M. Liedke, Phys. Rev. Lett. **90**, 097201 (2003).
[13] S. Ueda, Y. Iwasaki, Y. Uehara, and S. Ushioda, Phys. Rev. B **83**, 144424 (2011).
[14] K. Senapati, M. G. Blamire, and Z. H. Barber, Appl. Phys. Lett. **103**, 132406 (2013).
[15] F. Yildiz, M. Przybylski, and J. Kirschner, Phys. Rev. Lett. **103**, 147203 (2009).
[16] D. Backes, D. Bedau, H. Liu, J. Langer, and A. Kent, J. Appl. Phys. **111**, 07C721 (2012).
[17] Y. Wei, S. Akansel, T. Thersleff, I. Harward, R. Brucas, M. Ranjbar, S. Jana, P. Lansaker, Y. Pogoryelov, R. K. Dumas *et al.*, Appl. Phys. Lett. **106**, 042405 (2015).
[18] J. F. Cochran, J. Rudd, W. B. Muir, B. Heinrich, and Z. Celinski, Phys. Rev. B **42**, 508 (1990).
[19] S. M. Rezende, C. Chesman, M. A. Lucena, A. Azevedo, F. M. De Aguiar, and S. S. Parkin, J. Appl. Phys. **84**, 958 (1998).
[20] M. Belmeguenai, T. Martin, G. Woltersdorf, M. Maier, and G. Bayreuther, Phys. Rev. B **76**, 104414 (2007).
[21] H. Suhl, Phys. Rev. **97**, 555 (1955).
[22] J. Lindner, Z. Kollonitsch, E. Kosubek, M. Farle, and K. Baberschke, Phys. Rev. B **63**, 094413 (2001).
[23] Z. Zhang, L. Zhou, P. E. Wigen, and K. Ounadjela, Phys. Rev. B **50**, 6094 (1994).
[24] B. Heinrich and J. A. Bland, *Ultrathin Magnetic Structures II*, Vol. 3 (Springer, Berlin, 1994), pp. 195–222.
[25] J. B. Youssef and A. Layadi, J. Appl. Phys. **108**, 053913 (2010).
[26] A. Layadi, Phys. Rev. B **65**, 104422 (2002).
[27] B. Heinrich, Z. Celinski, J. F. Cochran, W. B. Muir, J. Rudd, Q. M. Zhong, A. S. Arrott, K. Myrtle, and J. Kirschner, Phys. Rev. Lett. **64**, 673 (1990).
[28] J. Lindner and K. Baberschke, J. Phys.: Condens. Matter **15**, S465 (2003).
[29] B. Aktas and F. Mikailzade, *Nanostructured Materials for Magnetoelectronics*, Vol. 175 (Springer Science & Business Media, New York, 2013).
[30] K. Lenz, T. Toliński, J. Lindner, E. Kosubek, and K. Baberschke, Phys. Rev. B **69**, 144422 (2004).
[31] D. A. Arena, E. Vescovo, C. C. Kao, Y. Guan, and W. E. Bailey, Phys. Rev. B **74**, 064409 (2006).
[32] Z. Zhang, L. Zhou, P. E. Wigen, and K. Ounadjela, Phys. Rev. Lett. **73**, 336 (1994).
[33] I. S. Maksymov and M. Kostylev, Physica E **69**, 253 (2015).
[34] Y. Wei, R. Brucas, K. Gunnarsson, Z. Celinski, and P. Svedlindh, Appl. Phys. Lett. **104**, 072404 (2014).
[35] Y. Wei, R. Brucas, K. Gunnarsson, I. Harward, Z. Celinski, and P. Svedlindh, J. Phys. D: Appl. Phys. **46**, 495002 (2013).
[36] J. Fassbender, F. Nörtemann, R. L. Stamps, R. E. Camley, B. Hillebrands, G. Güntherodt, and S. S. P. Parkin, Phys. Rev. B **46**, 5810(R) (1992).